P1.45 SCENE IDENTIFICATION FOR THE CERES CLOUD ANALYSIS SUBSYSTEM

Qing Trepte, Yan Chen, Sunny Sun-Mack
Science Applications International Corporation, Hampton, Virginia

Patrick Minnis*, David F. Young, Bryan A. Baum
Atmospheric Sciences, NASA Langley Research Center, Hampton, VA

Patrick W. Heck
Analytical Services and Materials, Inc., Hampton, VA

1. INTRODUCTION

Accurate measurement of the Earth's radiation budget and understanding of its interaction with various components of the atmosphere and surface requires reliable determination of the scene constituents. The Clouds and Earth's Radiant Energy System Project is meeting this need by simultaneously observing relatively low-resolution broadband radiances and high-resolution imager narrowband radiances. The latter are used to classify the scene while the former provide the radiation budget measurements. The scene classifications are used to help develop and select bidirectional reflectance models appropriate for the scene. Identification of the atmospheric state of each pixel facilitates further quantification of surface, aerosol, or cloud properties. This paper describes the methodology currently used by CERES for scene classification. Initial results are presented from an analysis of January 1998 Tropical Rainfall Measuring Mission (TRMM) satellite Visible Infrared Scanner (VIRS) data.

*Corresponding author address: Patrick Minnis, NASA Langley Research Center, MS 420, Hampton, VA 23681-2199. email: p.minnis@larc.nasa.gov.

2. METHODOLOGY

The CERES scene classification technique consists primarily of cascading threshold tests that use radiances taken at 0.65, 1.6, 3.7, 11, and 12 μm. To define a pixel as cloudy, at least, one of its five spectral radiances must differ significantly from the corresponding expected clear-sky radiances. A cloudy pixel may be classified as strong or weak depending on how much the radiances differ from the predicted clear-sky radiances. Pixels identified as clear are designated as weak or strong or categorized as being filled with smoke, fire, or aerosol, contaminated by sunglint, or covered with snow. The daytime (solar zenith angle, θ_o, < 78°) masking algorithm can use all five channels, while the nighttime technique only employs channels 3, 4, and 5. Predictions of clear radiances and their uncertainties are required to effect the scene classification. Although the clear radiances are estimated differently for each channel, each radiance must be specified for a given latitude λ, longitude ϕ, time of day t, month m, θ_o, viewing zenith angle θ, and relative azimuth angle ψ. Clear-sky radiances are predicted at a 10' latitude-longitude resolution, but are often only defined on a 1° grid. Each 10' box is defined as water, permanent snow, or land and has a mean altitude $z_s(\lambda,\phi)$ associated with it.

2.1 Daytime mask

Every pixel is classified during daylight using a sequence of tests as outlined in Fig. 1. The first check, or **A** test, identifies all pixels that are obviously too cold to be cloud free. If $T_4 < T_A$, then the pixel is designated a strong cloud. The value of T_A is equal to the temperature at 500 mb over land or to T_{skin} – 10K over ocean. If the pixel is not cloudy after the **A** test, it is then compared against the expected clear-sky radiances in the following **B** tests, where the parameters B1, B2, and B3 are initialized to 0.

1) If $T_4 < T_{cs4} - \sigma_4$, B1 = 1.

2) If $\rho_1 > \rho_{cs1}\,(1 + \sigma_1)$, B2 = 1.

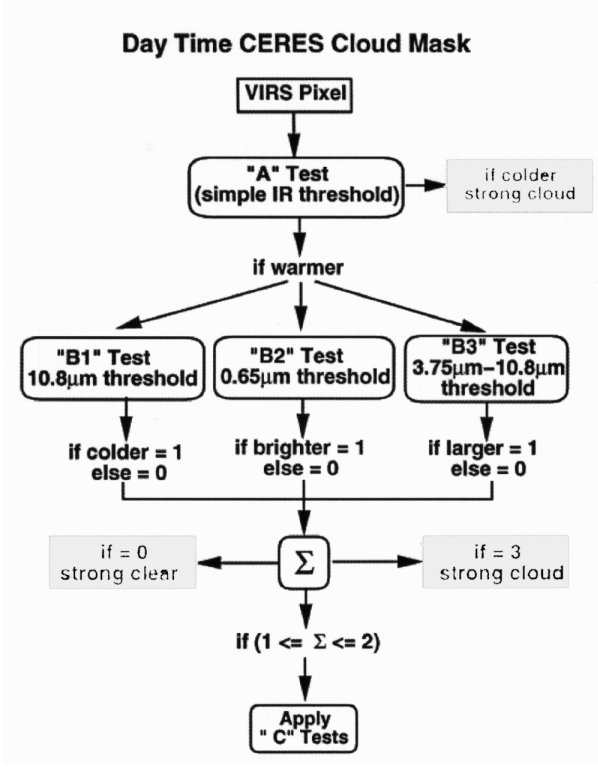

Fig. 1. Daytime CERES cloud mask algorithm.

3) If $T_3 - T_4 > T_{cs3} - T_{cs4} + \sigma_3$, B3 = 1.

The channel-1 observed and expected clear-sky reflectances are ρ_1 and ρ_{cs1}, respectively, while σ_1 is the uncertainty in ρ_{cs1}. The observed and expected brightness temperatures for channels 3 and 4 are T_3, T_4, T_{cs3}, and T_{cs4}, respectively. The corresponding clear-sky uncertainties are σ_3 and σ_4. If the sum of the **B** parameters is 0 or 1, then the pixel is classified as either strong clear or cloudy, respectively. Otherwise, a complicated set of **C** tests are then applied depending on the **B** tests that failed and the surface type. The **C** tests adjust the clear-sky uncertainties and may also involve channels 2 or 5. For example, if the scene is bright and cold over land, the **C** test will check for snow using the expected snow reflectance ratio of 0.65 to 1.6 μm. From these **C** tests, a pixel categorized as clear may be assigned additional classifiers such as strong, weak, snow, aerosol, smoke, fire, or glint. Cloudy pixels may be classified as strong, weak, glint, or multilayered.

2.2 Nighttime mask

The nighttime mask is similar as seen in Fig. 2. The **A** test is followed by **D** tests that begin

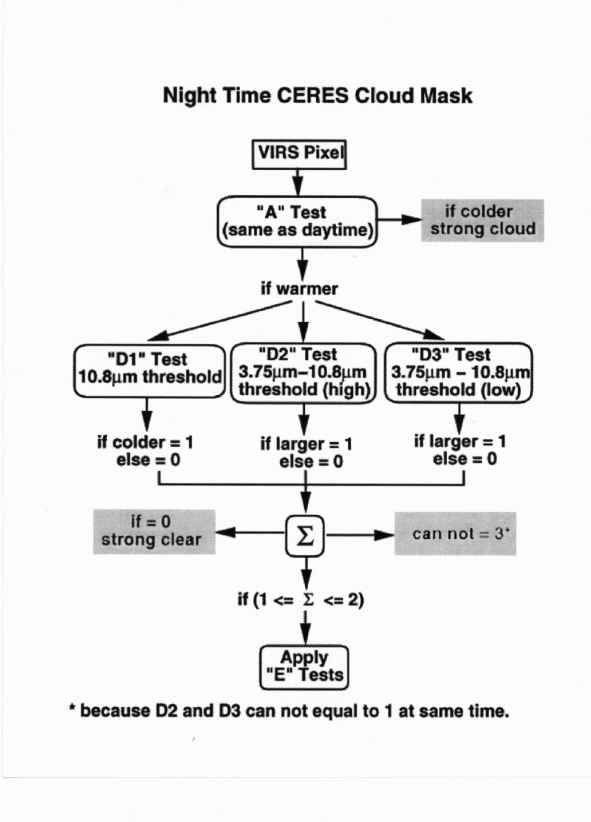

Fig. 2. CERES nighttime cloud mask algorithm.

with D1 = D2 = D3 = 0. The D1 and D2 tests are the same as B1 and B3, respectively. The D3 test checks determine if $T_3 - T_4 < T_{cs3} - T_{cs4} - \sigma_3$. If any of the **D** tests passes, then more complex **E** tests are applied that involve refined thresholds and channel 5. Otherwise, the pixel is classified as clear. The **E** tests will yield strong or weak clear or strong or weak cloudy classifications.

3. CLEAR-SKY RADIANCE DATA

Thresholds are determined empirically from a variety of sources and depend on the surface type. Clear-sky albedo maps, directional reflectance models, and bidirectional reflectance functions are used to predict expected clear-sky reflectances for the 0.65, 1.6, and 3.75-µm channels (e.g., Sun-Mack et al., 1999). The uncertainties used to define the thresholds are based on spatial and temporal standard deviations of the reflectances, uncertainties in the directional reflectance models, and variability within a 10' box. Surface altitude, vegetation type, snow coverage maps, and vertical profiles of temperature and humidity are all included the analysis procedures. Surface skin temperatures from numerical weather analyses and empirical spectral surface emissivities are used to compute top-of-atmosphere brightness temperatures at 3.75, 10.8, and 12.0 µm.

The channels-1 (visible) and -2 clear-sky reflectances are

$$\rho_1 = \alpha_1(\lambda,\phi,\mathrm{m})\ \delta_1(\theta_o)\ \chi_1(\theta_o,\theta,\Psi), \qquad (4)$$

where α_1 is the overhead-sun albedo, δ_1 is the normalized directional reflectance model, and χ_1 is the bidirectional distribution function (see Sun-Mack et al. 1999). Except for ocean, the values of δ_1 are defined for each of 19 IGBP (International Geosphere Biosphere Programme) surface types k from the results of Sun-Mack et al. (1999).

The clear-sky albedos and directional models for ocean are derived from an updated version of the clear ocean model of Minnis and Harrison (1984). The overhead-sun albedos for all other

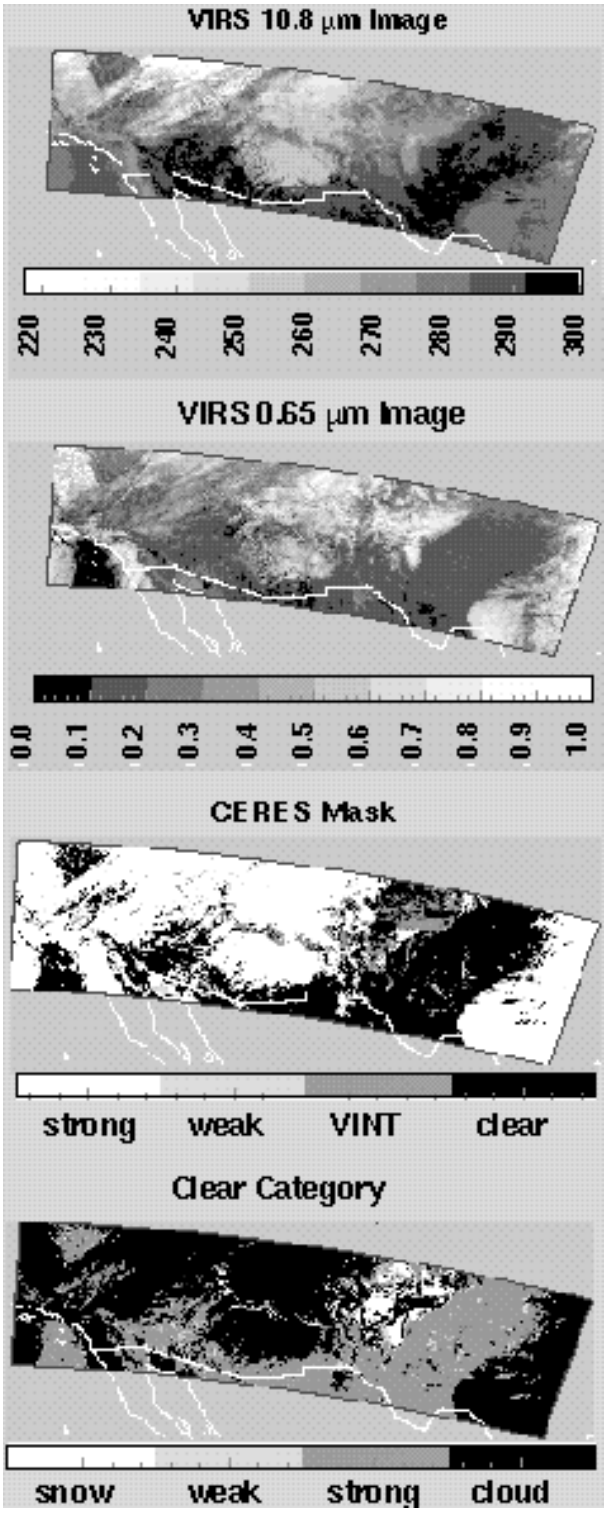

Fig. 3. Cloud mask results for VIRS image taken over the western USA at 1600 UTC, 1/16/99.

areas were taken from the maps created by Sun-Mack et al. (1999) using an initial pass through the VIRS data with the following procedure. Clear reflectances in a given 10' region are converted to α_1 using (4) and used to compute the mean and standard deviation for each pass during the month. The relative rms average $\sigma_1(\lambda,\phi,m)$ of the temporal and spatial standard deviations is normalized to $<\alpha_1>$ to obtain the basic uncertainty in a given value of $<\alpha_1>$. Mean values of α_1 (k,m) and σ_1(k,m) are then computed from the regions with data. The results for each month are filtered to eliminate poor sampling. All unfilled regions are then assigned the appropriate α_1(k,m) and σ_1(k,m). In application, (1) is solved using the filled dataset. If the observed clear-sky reflectances from the second passs through the VIRS data differ substantially from the initial results in a given 10' box, the albedo is updated to reflect the new observations. The result is a much more realistic 10' overhead visible albedo.

The 1.6-µm albedos are based on an initial pass through the VIRS data. Their derivation is described by Sun-Mack et al. (1999). The surface reflectances are computed in a fashion similar to (4) then adjusted to the top of the atmosphere (TOA) by accounting for gaseous absorption. These results are also updated when the observed values differ significantly from the original predicted values.

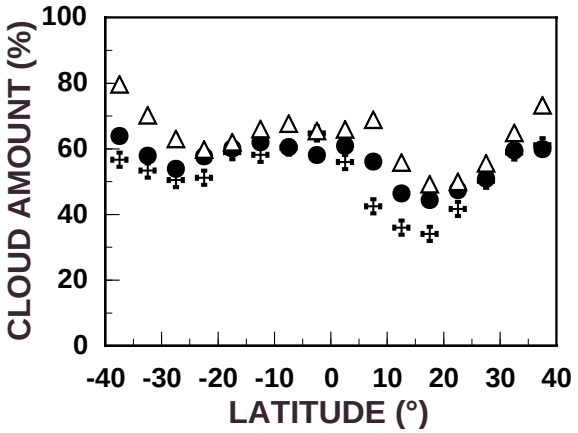

Fig. 4. Mean January cloud amounts from surface (1971-81; ●), ISCCP D product (1986-93; △), VIRS (1998; ✣).

The 3.7-µm radiance leaving the surface is approximated as

$$B_3(T_{s3}) = \varepsilon_3\{B_3(T_{skin})\} + \alpha_3\, \delta_3(\theta_o)\, \chi_3 S_3', \qquad (2)$$

where B_3 is the Planck function, T_{skin} is the surface skin temperature, ε_3 is the surface emissivity, T_{s3} is the apparent surface temperature at 3.7 µm, and S_3' is the solar radiation incident at the surface. $B_3(T_{s3})$ is then corrected for attenuation by the atmosphere to predict the clear-sky temperature T_{cs3}. The surface emissivities for channels 3, 4, and 5 were derived from the clear-sky ISCCP DX (ISCCP refers to the International Satellite Cloud Climatology Project, Rossow and Schiffer, 1991) data on a 1° grid using the method described by Minnis et al. (1998). Means and standard deviations are computed and all 1° regions with no emissivities are filled using the IGBP-type averages. The values of δ_3 and χ_3 are specified using δ_1 and χ_1, respectively. This approach yields a mean difference between the observed and predicted values of T_{cs3} of –2 to +2K and –1 to +1K during daytime and nighttime, respectively, with standard deviations σ_3 less than 3K and 2K.

The 10.8 and 12.0-µm TOA temperatures are derived from 3-hourly skin temperatures computed by a numerical weather analysis model and corrected for temporal phase lags and the surface emissivity. The temperatures are then adjusted to the TOA accounting for gaseous absorption and emission of the atmosphere. Clear-sky temperature uncertainties are estimated as the standard deviations between the predicted and observed temperatures. A minimum of 2.5 K is set for ocean and 3.0K for land.

4. RESULTS & CONCLUDING REMARKS

The masks were applied to VIRS data taken during January 1998 between 38°S and 38°N. Figure 3 shows a daytime VIRS scene over the southwestern USA, where snow was present in many areas. Most of the pixels were classified as good clear or cloudy. For the month, the mean daytime cloud fraction was 50.9% compared to 53.3% at night for a mean of 52.2%. Over land and ocean, respectively, the mean cloud amounts were 46.1 and 54.5%. No significant day-night difference was found over land, while mean cloud amounts were 56.5% and 52.5% during day and night, respectively, over the oceans.

The zonal means shown in Fig. 4 show patterns very similar to those from surface (Warren et al., 1986, 1988) mean is 56.3%) and the ISCCP (mean is 63.6%) climatologies. The mean VIRS values, however, are 4 and 11% less than the respective surface and ISCCP means.

The CERES mask is subject to further improvement as more clear-sky and bidirectional reflectance data become available. Validation efforts are underway. The initial results are quite reasonable and will aid the development of improved cloud anisotropic models and serve as a basis for understanding the relationship between cloud properties and the radiation budget.

References

Minnis, P. and E. F. Harrison, 1984: Diurnal variability of regional cloud and clear-sky radiative parameters derived from GOES data. Part III: November 1978 radiative parameters. J. Clim. Appl. Meteor., **23**, 1032-1052.

Minnis, P., W. L. Smith, Jr., and D. F. Young, 1998: Surface emissivity derived from multispectral satellite data. Proc. 8th Ann. ARM Science Team Mtg., Tuscon, AZ, March 23-27, 489-494.

Sun-Mack, S., Y. Chen, T. D. Murray, P. Minnis, and D. F. Young, 1999: Visible clear-sky and near-infrared surface albedos derived from VIRS data for CERES. Proc. AMS 10th Conf. Atmos. Rad., Madison, WI, June 28-July 2.

Rossow, W. B. and R. A. Schiffer, 1991: ISCCP cloud data products. Bull. Am. Meteor. Soc., **72**, 2-20.

Warren, S.G., C.J. Hahn, J. London, R.M. Chervin, and R.L. Jenne, Global distribution of total cloud cover and cloud type amounts over land. NCAR Tech. Note NCAR/TN-273+STR, 229 pp., 1986

Warren, S.G., C. J. Hahn, J. London, R.M. Chervin, and R. L. Jenne, 1988: Global distribution of total cloud cover and cloud type amounts over ocean. NCAR Tech. Note NCAR/TN-317+STR, 212 pp.